nature geoscience

Supplementary information

https://doi.org/10.1038/s41561-024-01537-8

Indo-Pacific regional extremes aggravated by changes in tropical weather patterns

In the format provided by the authors and unedited

Contents

1 Sensitivity study of the trend analysis

We carried out an extensive sensitivity study of our trend-analysis results. In the manuscript, we report the sensitivity study of the results with respect to (i) the observable used – Extended Data Figs. 2 and 3, (ii) the number of time periods adopted for trend analysis – Extended Data Fig. 4, (iii) the satellite observation era – Extended Data Fig. 7, and (iv) the reanalysis dataset – Figs. 5 and 6.

Here, we report further sensitivity results with respect to (iv) the reanalysis dataset, where we used JRA55 reanalysis data (Supplementary Fig. 1), and 20CR (Supplementary Fig. 2), and with respect to (v) the dimensions of the domain (Supplementary Fig. 3), where we used the extended domain 30°S to 30°N (instead of 20°S to 20°N). These three additional figures have been obtained for a number of bin equal to 9, as the reference results obtained on ERA5 data. The results across these reanalysis datasets are consistent with the initial findings obtained on ERA5, further supporting the analysis and conclusions.

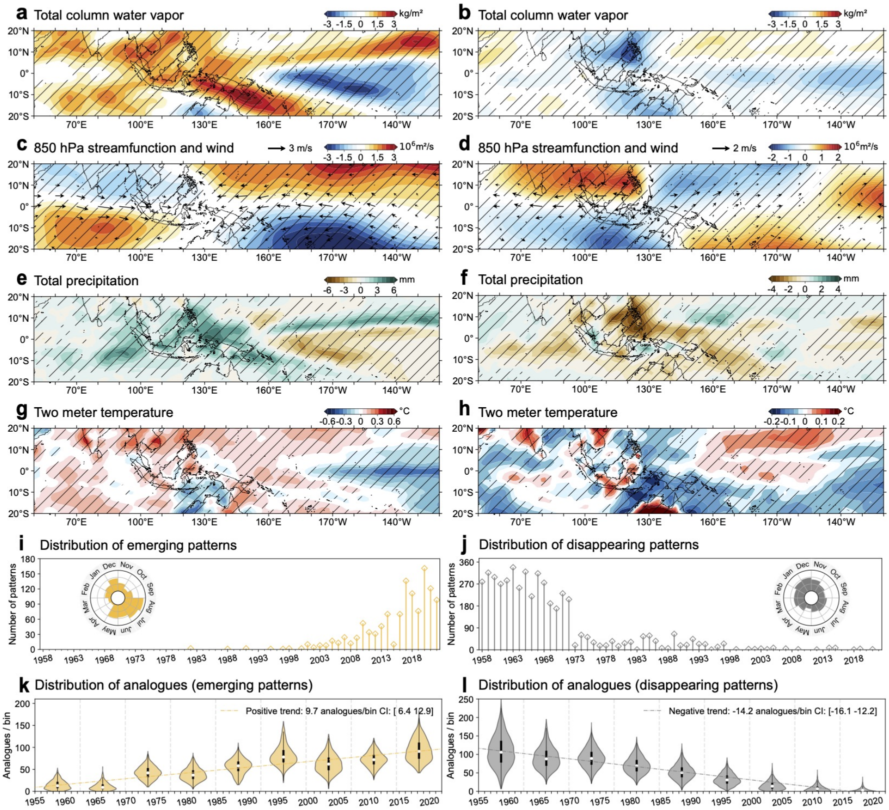

Supplementary Fig. 1: **Composite anomalies (a–h), for patterns with significant occurrence trends (i,j), and associated analogues (k,l), using TCWV as observable**. As in Fig. 1, but for the JRA55 reanalysis dataset.

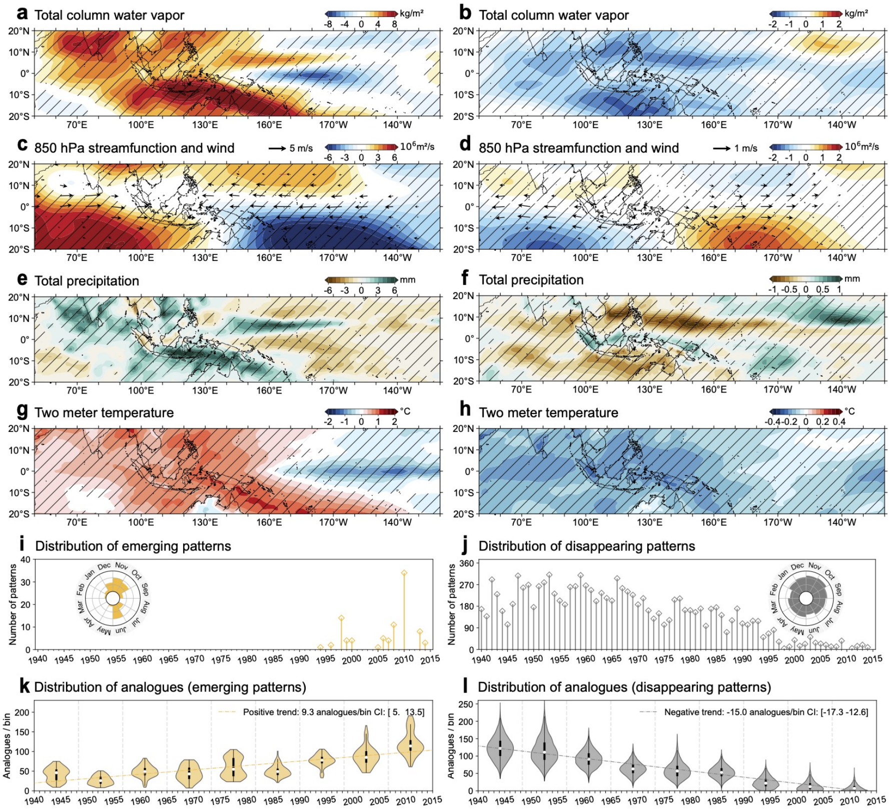

Supplementary Fig. 2: **Composite anomalies (a–h), for patterns with significant occurrence trends (i,j), and associated analogues (k,l)**. As in Fig. 1, but for the 20CR reanalysis dataset.

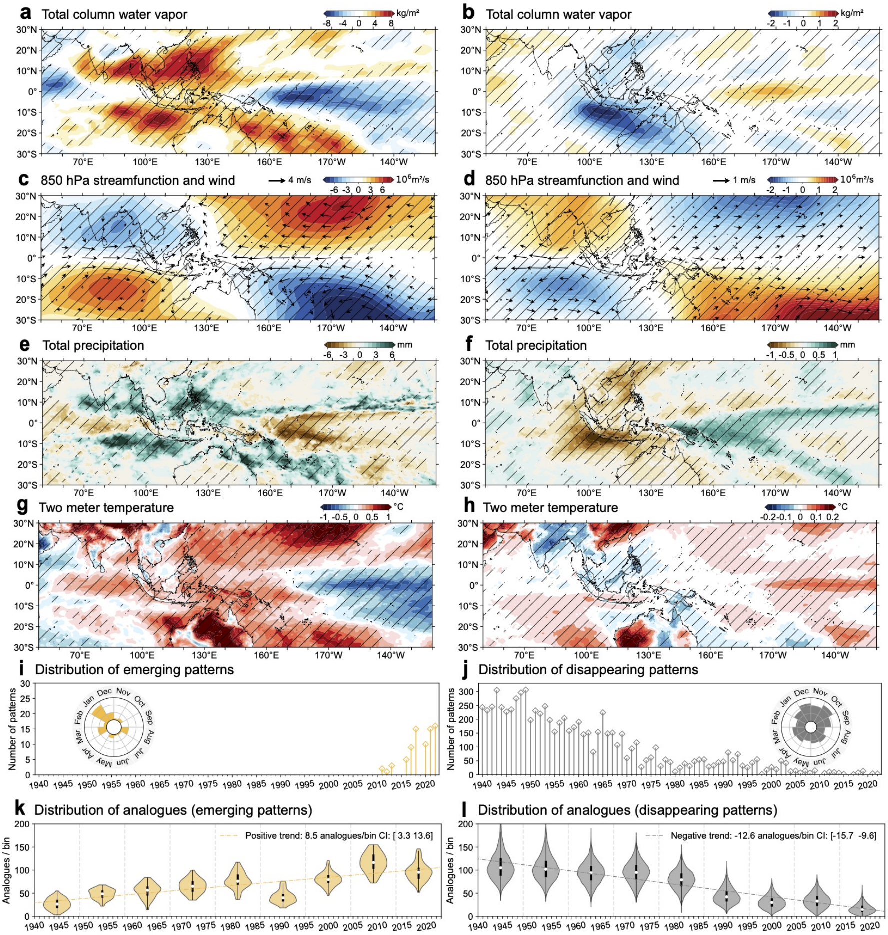

Supplementary Fig. 3: **Composite anomalies (a–h), for patterns with significant occurrence trends (i,j), and associated analogues (k,l)**. As in Fig. 1, but using the extended domain 30°S to 30°N.

2 Frequency maps and EM-DAT results for the other three seasons: MAM, JJA, and SON

In the manuscript, we report extreme weather frequency maps for the DJF (December, January, February) season. Here, we report the results for all other seasons, namely MAM (March, April, May) – Supplementary Fig. 4, JJA

(June, July, August) – Supplementary Fig. 5, and SON (September, October, November) – Supplementary Fig. 6. We also report the frequency maps for the entire year, without separating it by seasons – Supplementary Fig. 7. These results supports the findings presented in the manuscript, highlighting an increased frequency of extreme weather for the emerging patterns identified, across the other three seasons.

In Supplementary Figs. 8, 9, and 10, we additionally show the results for the EM-DAT analysis (same as Fig. 3 in the manuscript), for MAM, JJA, and SON, respectively. The results are consistent with the findings obtained in the manuscript.

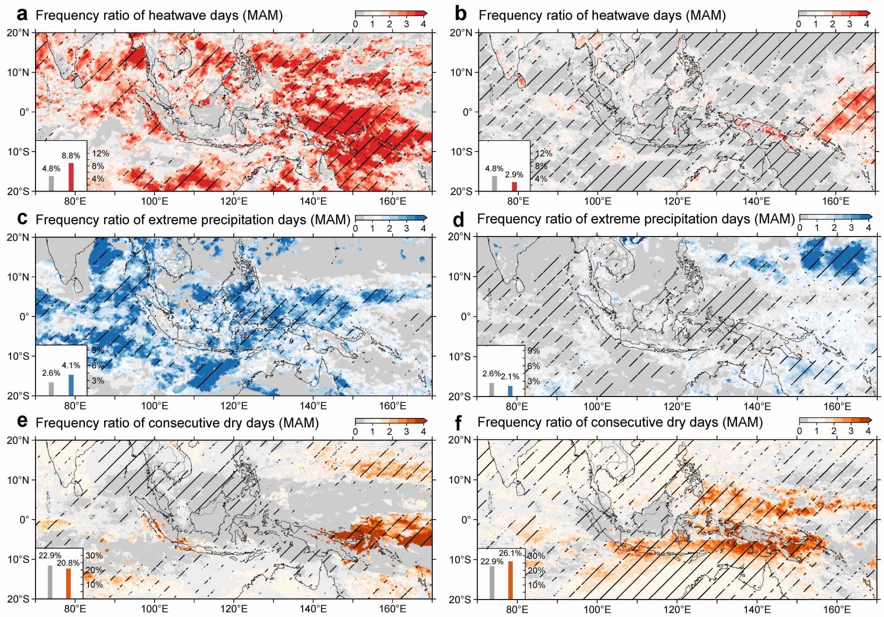

Supplementary Fig. 4: **Weather extremes associated with emerging (a,c,e) and disappearing (b,d,f) weather patterns in MAM**. Frequency ratio maps for heatwaves (a,b), extreme precipitation (c,d), and consecutive dry days (e,f). Diagonal black lines indicate regions with changes that are statistically significant at the one-sided 5% level, computed with a bootstrap sample size of 500. Same as Fig. 2, but for MAM (March-April-May).

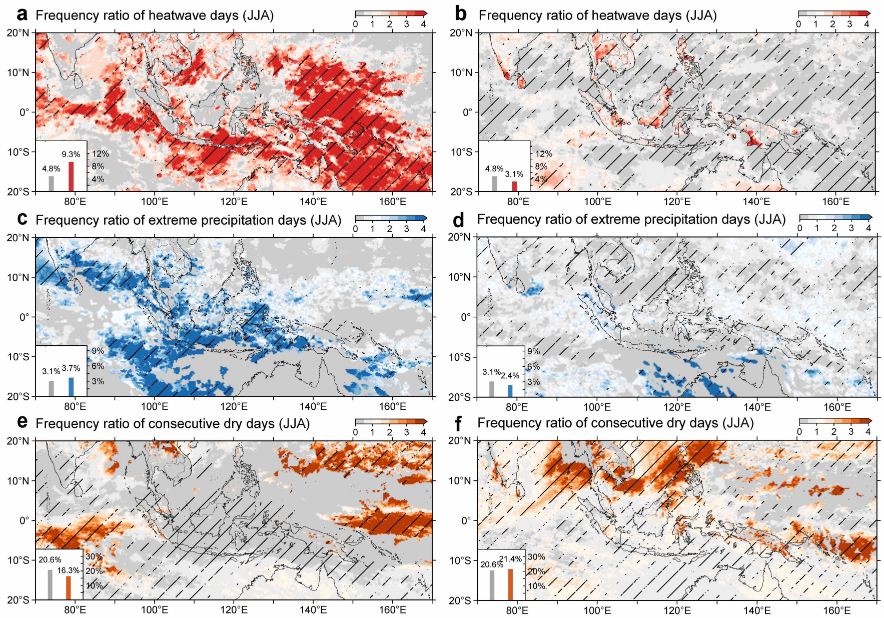

Supplementary Fig. 5: **Weather extremes associated with emerging (a,c,e) and disappearing (b,d,f) weather patterns in JJA**. Frequency ratio maps for heatwaves (a,b), extreme precipitation (c,d), and consecutive dry days (e,f). Diagonal black lines indicate regions with changes that are statistically significant at the one-sided 5% level, computed with a bootstrap sample size of 500. Same as Fig. 2, but for JJA (June-July-August).

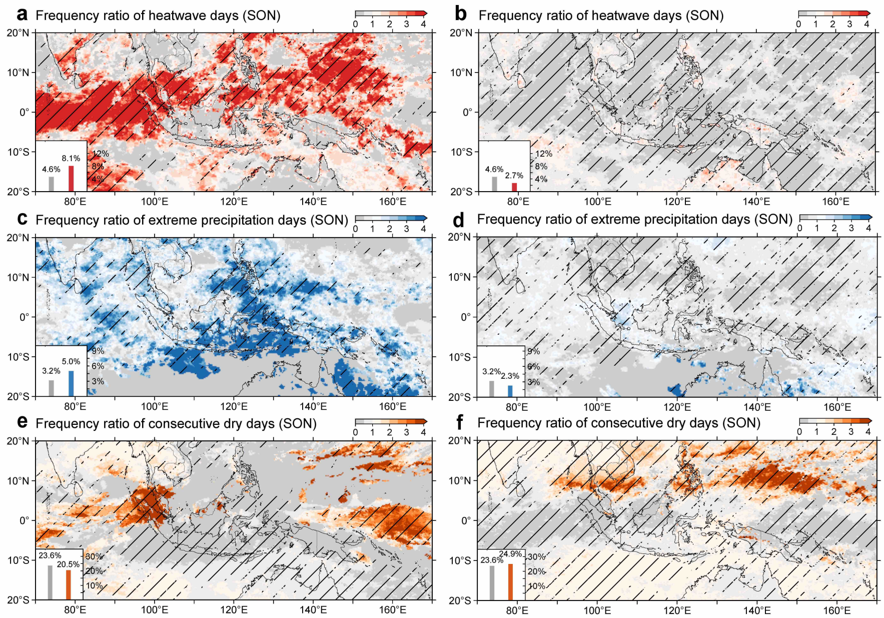

Supplementary Fig. 6: **Weather extremes associated with emerging (a,c,e) and disappearing (b,d,f) weather patterns in SON**. Frequency ratio maps for heatwaves (a,b), extreme precipitation (c,d), and consecutive dry days (e,f). Diagonal black lines indicate regions with changes that are statistically significant at the one-sided 5% level, computed with a bootstrap sample size of 500. Same as Fig. 2, but for SON (September-October-November).

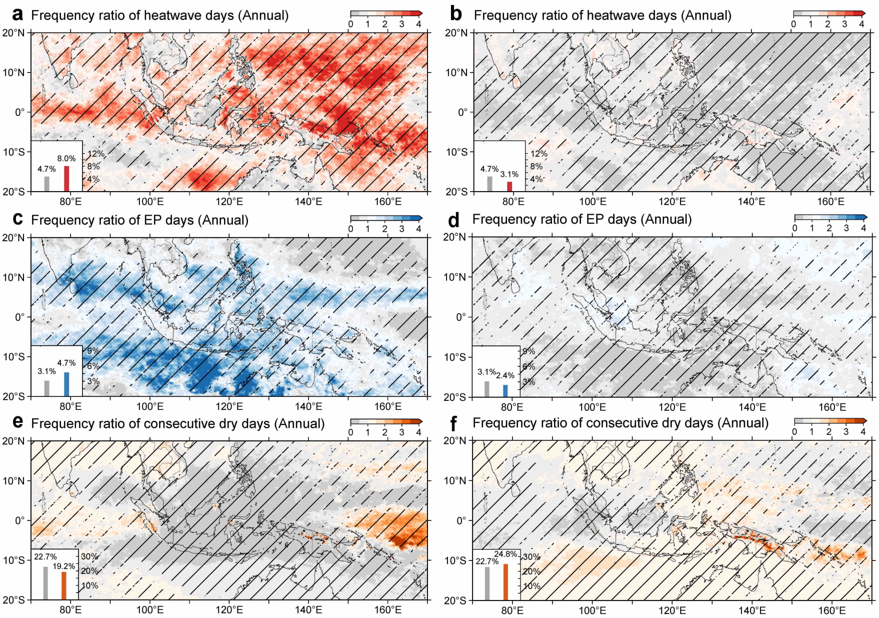

Supplementary Fig. 7: **Weather extremes associated with emerging (a,c,e) and disappearing (b,d,f) weather patterns in all seasons**. Frequency ratio maps for heatwaves (a,b), extreme precipitation (c,d), and consecutive dry days (e,f). Diagonal black lines indicate regions with changes that are statistically significant at the one-sided 5% level, computed with a bootstrap sample size of 500. Same as Fig. 2, but for all seasons.

a EM-DAT floods (MAM)

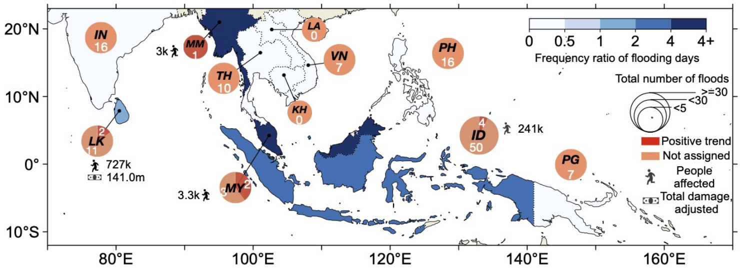

b Flooding days from EM-DAT (MAM)

	All countries	TH	PH	VN	LK	MY	ID	IN	PG	KH	MM	LA
Flooding Days	485 (12.0%)	49 (1.2%)	48 (1.2%)	25 (0.6%)	74 (1.8%)	23 (0.6%)	231 (5.7%)	80 (2.0%)	32 (0.8%)	0	7 (0.2%)	0
Flooding Days (Emerging)	13 (23.2%)	0	0	0	2 (3.6%)	3 (5.4%)	7 (12.5%)	0	0	0	2 (3.6%)	0
Frequency Ratio	1.94	0	0	0	1.95	9.43	2.19	0	0	—	20.65	—

*Total number of MAM days (1979-2022): 4048, Emerging patterns: 56

Supplementary Fig. 8: **Impact of emerging weather patterns over the tropical Indo-Pacific region according to floods recorded in the EM-DAT database**. The choropleth map in plot (a) depicts the ratio of flood days recorded under changing weather patterns, compared to climatology. The sizes of the pie charts represent the total floods per country from 1979-2022, with red slices representing floods linked to emerging weather patterns and orange slices for those not assigned. The table in plot (b) shows the total number of flooding days within the MAM season for each country (first row), the flood days associated with emerging weather patterns (second row), and the respective frequency ratios (third row).

a EM-DAT floods (JJA)

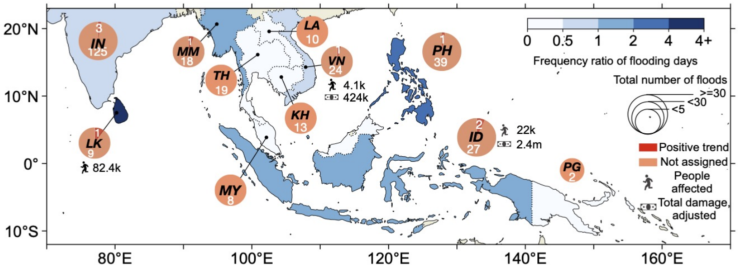

b Flooding days from EM-DAT (JJA)

	All countries	TH	PH	VN	LK	MY	ID	IN	PG	KH	MM	LA
Flooding Days	1235 (30.5%)	128 (3.2%)	164 (4.1%)	132 (3.3%)	43 (1.1%)	29 (0.7%)	105 (2.6%)	675 (16.7%)	2 (0.04%)	98 (2.4%)	130 (3.2%)	62 (1.5%)
Flooding Days (Emerging)	15 (37.5%)	0	4 (10.3%)	1 (2.6%)	2 (5.1%)	0	2 (5.1%)	5 (12.8%)	0	0	2 (5.1%)	0
Frequency Ratio	1.26	0	2.53	0.79	4.83	0	1.98	0.77	0	0	1.60	0

*Total number of JJA days (1979-2022): 4048, Emerging patterns: 39

Supplementary Fig. 9: **Impact of emerging weather patterns over the tropical Indo-Pacific region according to floods recorded in the EM-DAT database**. The choropleth map in plot (a) depicts the ratio of flood days recorded under changing weather patterns, compared to climatology. The sizes of the pie charts represent the total floods per country from 1979-2022, with red slices representing floods linked to emerging weather patterns and orange slices for those not assigned. The table in plot (b) shows the total number of flooding days within the JJA season for each country (first row), the flood days associated with emerging weather patterns (second row), and the respective frequency ratios (third row).

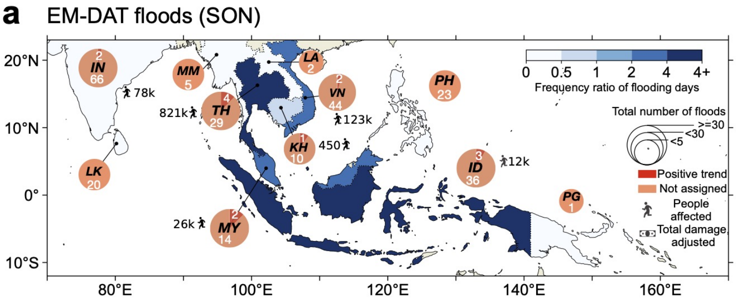

b Flooding days from EM-DAT (SON)

	All countries	TH	PH	VN	LK	MY	ID	IN	PG	KH	MM	LA
Flooding Days	1057 (26.4%)	182 (4.5%)	99 (2.5%)	282 (7.0%)	132 (3.3%)	82 (2.0%)	150 (3.7%)	393 (9.8%)	10 (0.2%)	83 (2.1%)	16 (0.4%)	11 (0.3%)
Flooding Days (Emerging)	25 (45.5%)	12 (21.8%)	0	9 (16.3%)	0	4 (7.3%)	11 (20.0%)	2 (3.6%)	0	1 (1.8%)	0	0
Frequency Ratio	1.72	4.8	0	2.32	0	3.55	5.34	0.37	0	0.88	0	0

*Total number of SON days (1979-2022): 4048, Emerging patterns: 55

Supplementary Fig. 10: Impact of emerging weather patterns over the tropical Indo-Pacific region according to floods recorded in the EM-DAT database. The choropleth map in plot (a) depicts the ratio of flood days recorded under changing weather patterns, compared to climatology. The sizes of the pie charts represent the total floods per country from 1979-2022, with red slices representing floods linked to emerging weather patterns and orange slices for those not assigned. The table in plot (b) shows the total number of flooding days within the SON season for each country (first row), the flood days associated with emerging weather patterns (second row), and the respective frequency ratios (third row).

3 Role of variability on weather extremes for the three other seasons: MAM, JJA, and SON

In the manuscript, we use pie charts to understand the role of internal variability for the DJF (December, January, February) season, where we focused on ENSO. Here, we report the results for all other seasons, namely MAM (March, April, May) – Supplementary Fig. 11, JJA (June, July, August) – Supplementary Fig. 12, and SON (September, October, November) – Supplementary Fig. 13. These results supports the findings presented in the manuscript, (related to Fig. 4), and highlight a substantial contribution of the emerging patterns identified to extreme weather conditions in the region.

3.1 ENSO-driven variability

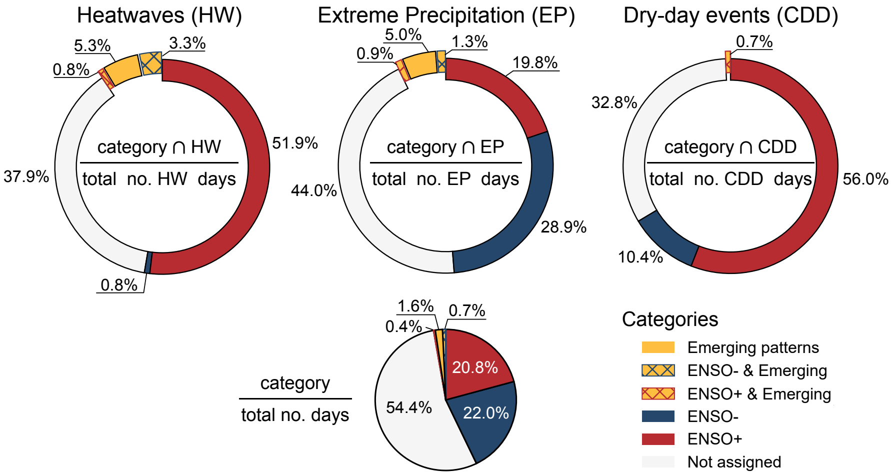

Supplementary Fig. 11: **Comparative analysis of extreme weather across ENSO phases and emerging patterns in MAM**. As in Fig. 4 but for MAM.

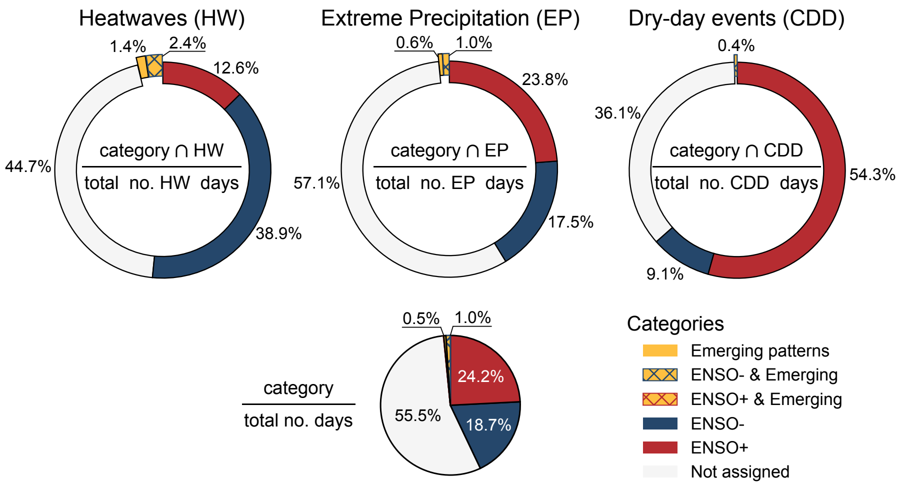

Supplementary Fig. 12: Comparative analysis of extreme weather across ENSO phases and emerging patterns in JJA. As in Fig. 4 but for JJA.

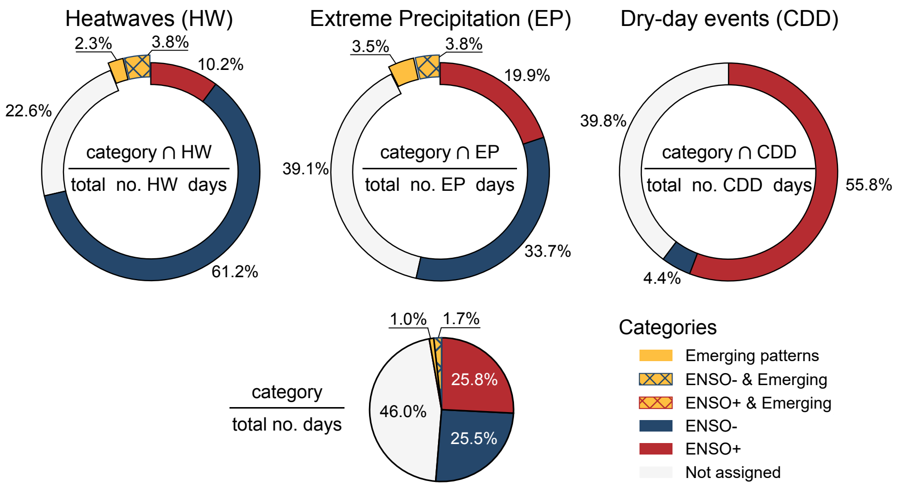

Supplementary Fig. 13: Comparative analysis of extreme weather across ENSO phases and emerging patterns in SON. As in Fig. 4 but for SON.

3.2 IOD-driven variability

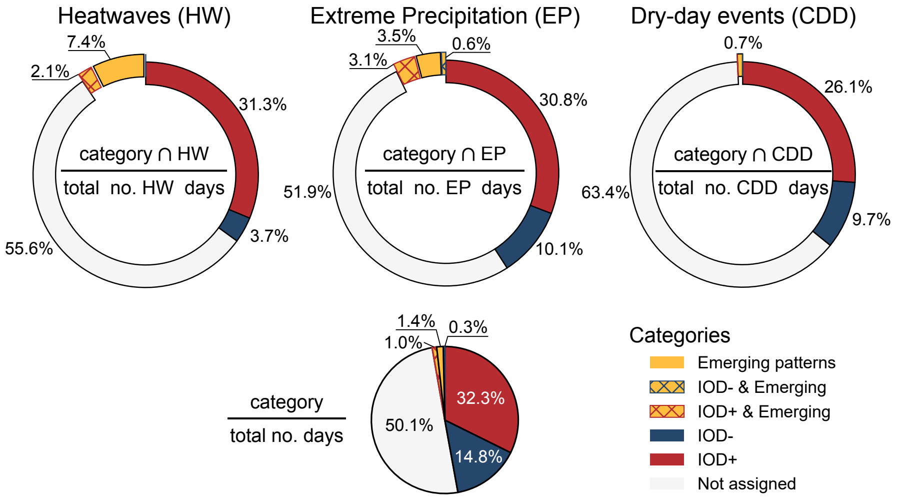

Supplementary Fig. 14: Comparative analysis of extreme weather across IOD phases and emerging patterns in MAM. As in Fig. 4 but for IOD, in MAM.

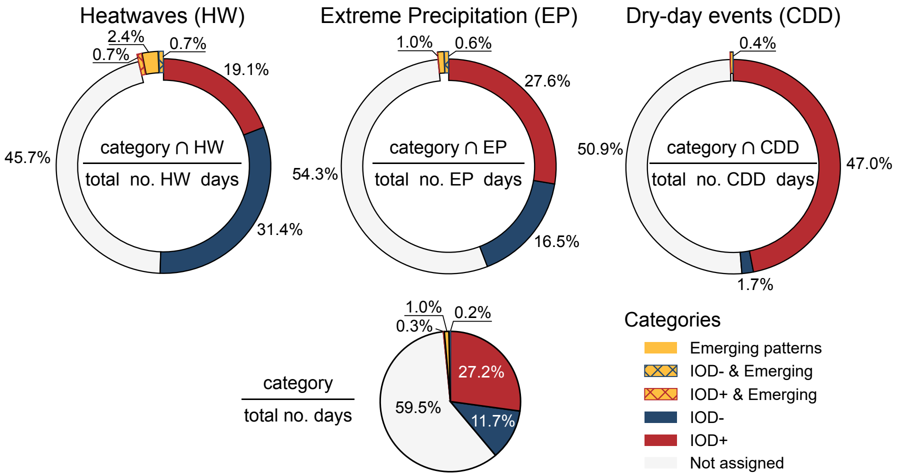

Supplementary Fig. 15: Comparative analysis of extreme weather across IOD phases and emerging patterns in JJA. As in Fig. 4 but for IOD, in JJA.

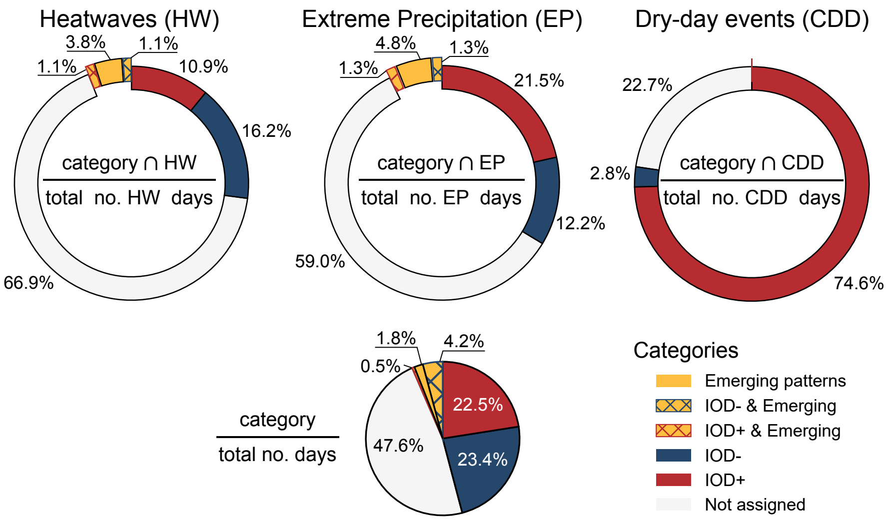

Supplementary Fig. 16: **Comparative analysis of extreme weather across IOD phases and emerging patterns in SON**. As in Fig. 4 but for IOD, in SON.

3.3 PDO-driven variability

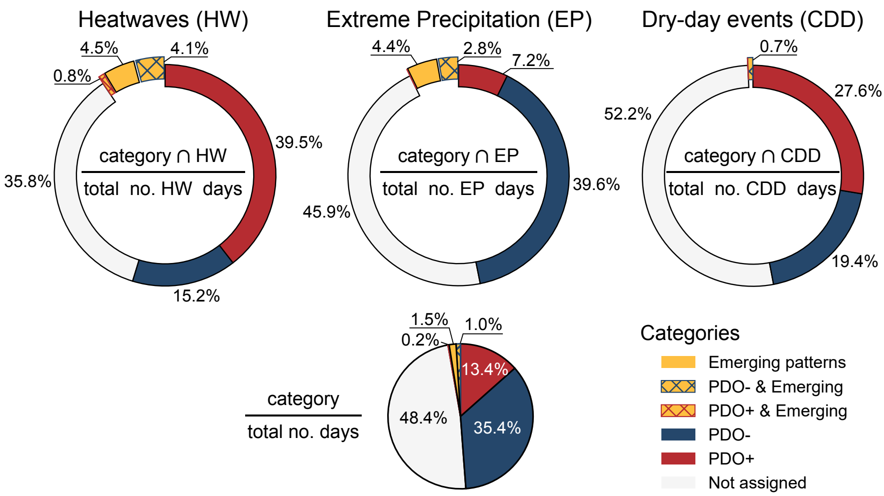

Supplementary Fig. 17: **Comparative analysis of extreme weather across PDO phases and emerging patterns in MAM**. As in Fig. 4 but for PDO, in MAM.

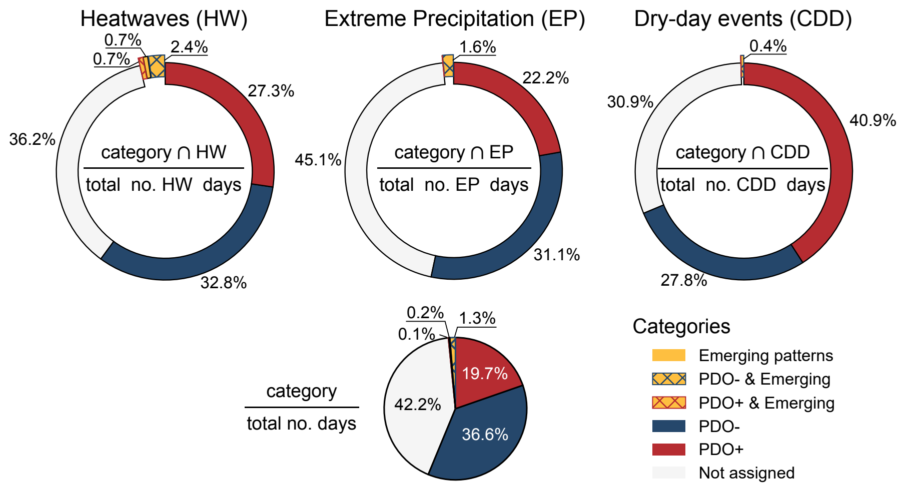

Supplementary Fig. 18: Comparative analysis of extreme weather across PDO phases and emerging patterns in JJA. As in Fig. 4 but for PDO, in JJA.

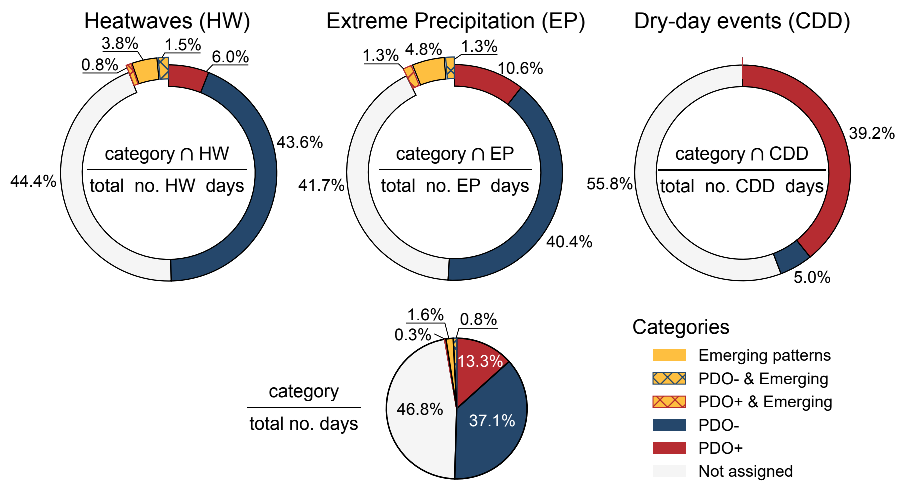

Supplementary Fig. 19: Comparative analysis of extreme weather across PDO phases and emerging patterns in SON. As in Fig. 4 but for PDO, in SON.

3.4 AMO-driven variability

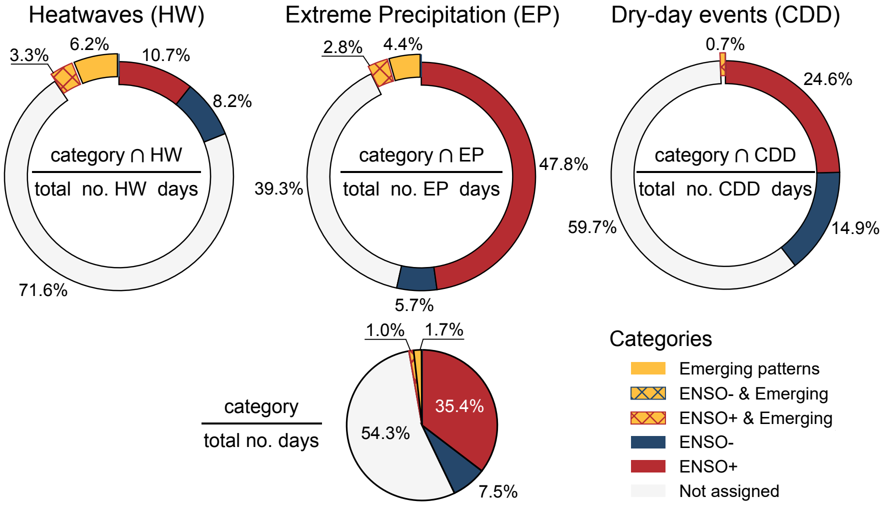

Supplementary Fig. 20: **Comparative analysis of extreme weather across AMO phases and emerging patterns in MAM**. As in Fig. 4 but for AMO, in MAM.

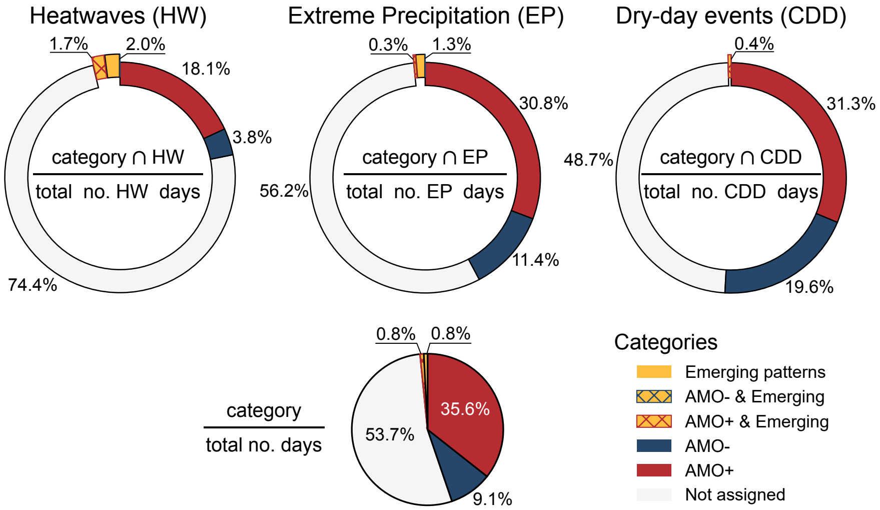

Supplementary Fig. 21: **Comparative analysis of extreme weather across AMO phases and emerging patterns in JJA**. As in Fig. 4 but for AMO, in JJA.

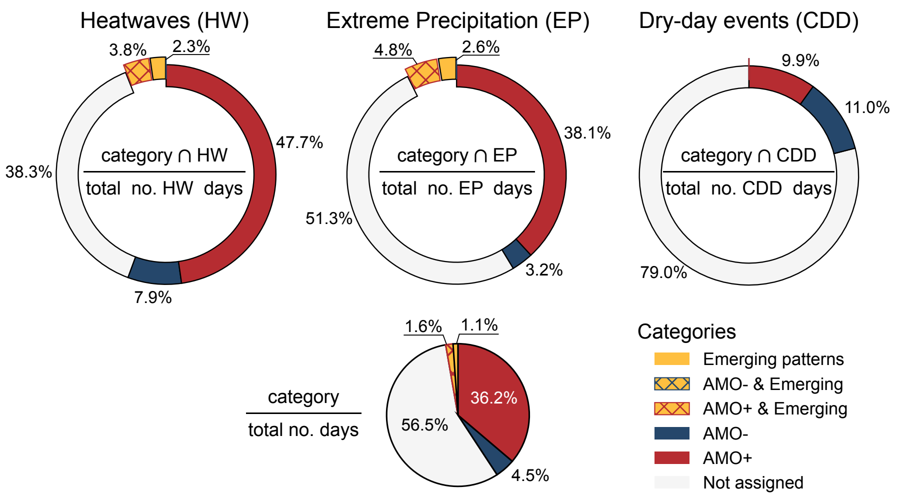

Supplementary Fig. 22: Comparative analysis of extreme weather across AMO phases and emerging patterns in SON. As in Fig. 4 but for AMO, in SON.

4 Distribution of identified patterns with respect to modes of variability

In this section, we present violin plots showing the distribution of both emerging and disappearing patterns with respect to the modes of variability considered, namely ENSO, IOD, PDO, and AMO. We present two figures. The first, figure 23, uses quantile-based thresholds for identifying positive, negative, and neutral phases of each mode of variability. This approach is used in a number of papers in the literature [1–3]. This approach is used to obtain the frequency maps in Supplementary Information section 5. The second, figure 24, uses absolute thresholds for for identifying positive, negative, and neutral phases of each mode of variability. This approach is used in a number of papers in the literature [4–6].

For the quantile-based threshold approach (Supplementary Fig. 23), we note that that the mean value (dot in the violin plots) for all data (white), emerging patterns (yellow violin plot) and disappearing patterns (grey violin plot) is mostly in the neutral phase of each mode, except for the emerging patterns vs AMO. In this case, the emerging patterns are slightly above the threshold, that indicates weak positive AMO conditions.

For the absolute threshold approach (Supplementary Fig. 24), we note that that the mean value (dot in the violin plots) for all data (white), emerging patterns (yellow violin plot) and disappearing patterns (grey violin plot) is mostly in the neutral phase of each mode, except for the emerging patterns vs ENSO. In this case, the emerging patterns are slightly below the threshold, that indicates weak La Niña conditions.

Remarkably, if we condition extreme weather with respect to mode of variability phases obtained using quantile-based thresholds, as done in Supplementary Information section 5, we are unable to reproduce increased frequency of extremes as high as the one obtained for the emerging patterns identified in this work. This indicates that the variability mode phase, while it contributes to modulating extreme weather, it is unable to fully explain the increased frequency seen for the emerging patterns. Hence, emerging patterns and the changing dynamics of the tropical Indo-Pacific are playing a key role.

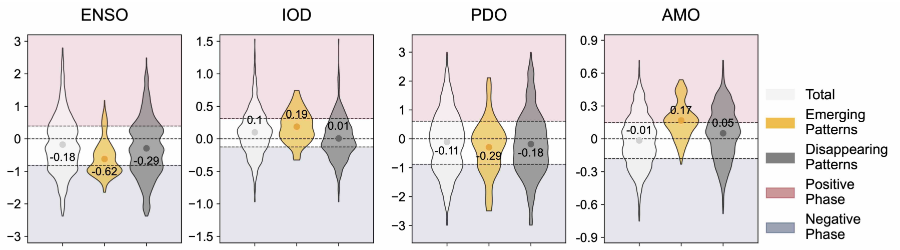

Supplementary Fig. 23: **Violin plots showing patterns vs modes of variability phases using quantile-based thresholds**. The shaded red and blue areas indicate positive and negative phase of each mode of variability obtained using the quantile-based thresholds, while the white area indicate neutral phase. The three violin plots correspond to all data available (white), to the emerging patterns (yellow), and to the disappearing patterns (grey). The dot in each violin plot corresponds to the mean value.

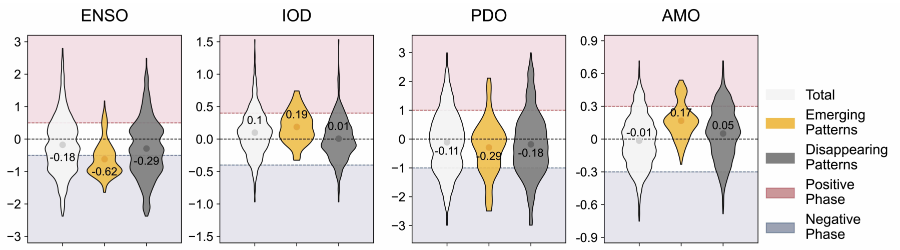

Supplementary Fig. 24: **Violin plots showing patterns vs modes of variability phases using absolute thresholds**. The shaded red and blue areas indicate positive and negative phase of each mode of variability obtained using absolute thresholds, while the white area indicate neutral phase. The three violin plots correspond to all data available (white), to the emerging patterns (yellow), and to the disappearing patterns (grey). The dot in each violin plot corresponds to the mean value.

5 Frequency maps conditioned to modes of variability

In this section, we present the frequency ratio maps, identical to Fig. 2 in the main manuscript, but obtained conditioning extremes with respect to mode of variability phases computed using the quantile-based thresholds presented in Supplementary Fig. 23. Remarkably, all the results presented in this section are unable to reproduce an increased frequency of heatwaves and extreme precipitation as significant the one obtained for the emerging patterns identified in this work.

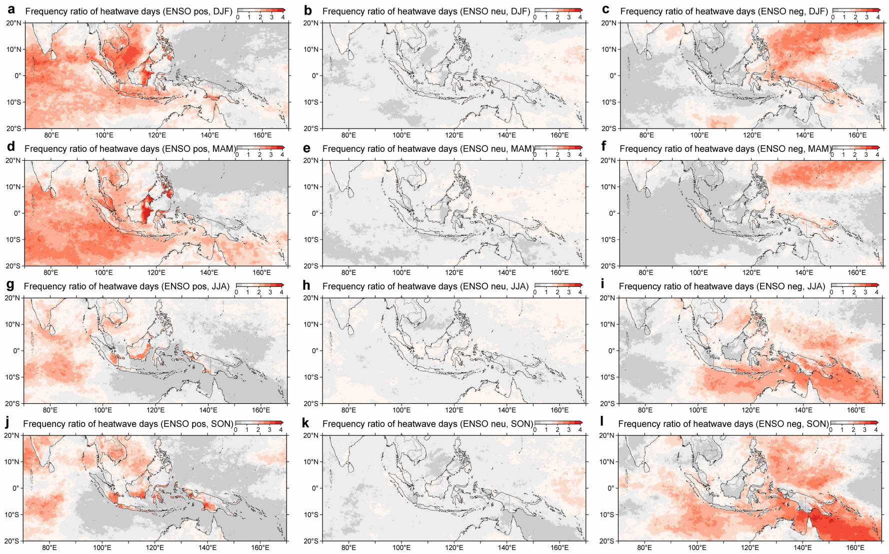

Supplementary Fig. 25: **Frequency ratio maps of heatwaves conditioned to different ENSO phases**. The positive, negative and neutral phases were obtained using the quantile-based thresholds presented in Supplementary Information section 4.

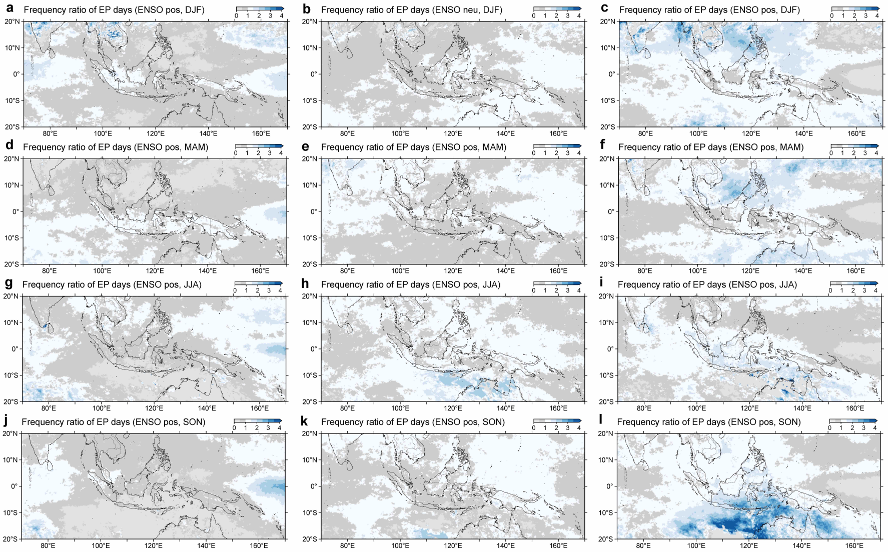

Supplementary Fig. 26: **Frequency ratio maps of extreme precipitation conditioned to different ENSO phases**. The positive, negative and neutral phases were obtained using the quantile-based thresholds presented in Supplementary Information section 4.

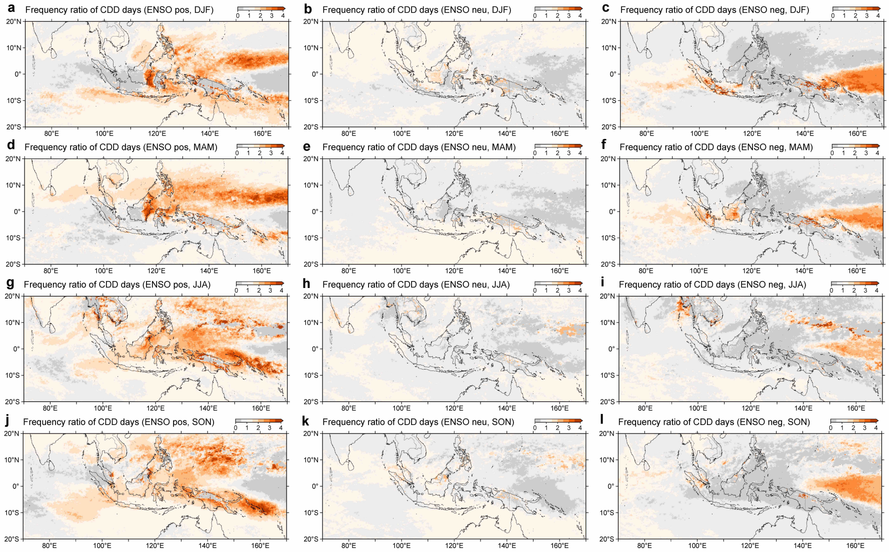

Supplementary Fig. 27: **Frequency ratio maps of consecutive dry days conditioned to different ENSO phases**. The positive, negative and neutral phases were obtained using the quantile-based thresholds presented in Supplementary Information section 4.

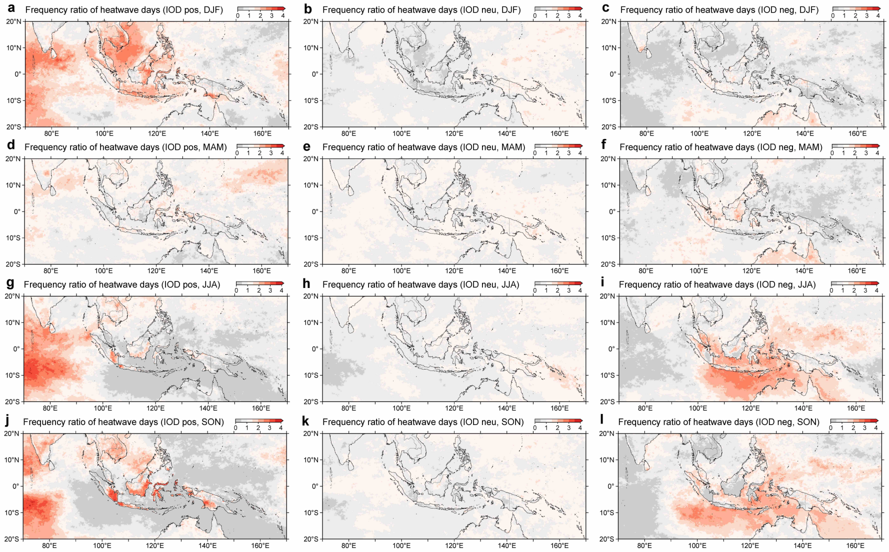

Supplementary Fig. 28: **Frequency ratio maps of heatwaves conditioned to different IOD phases**. The positive, negative and neutral phases were obtained using the quantile-based thresholds presented in Supplementary Information section 4.

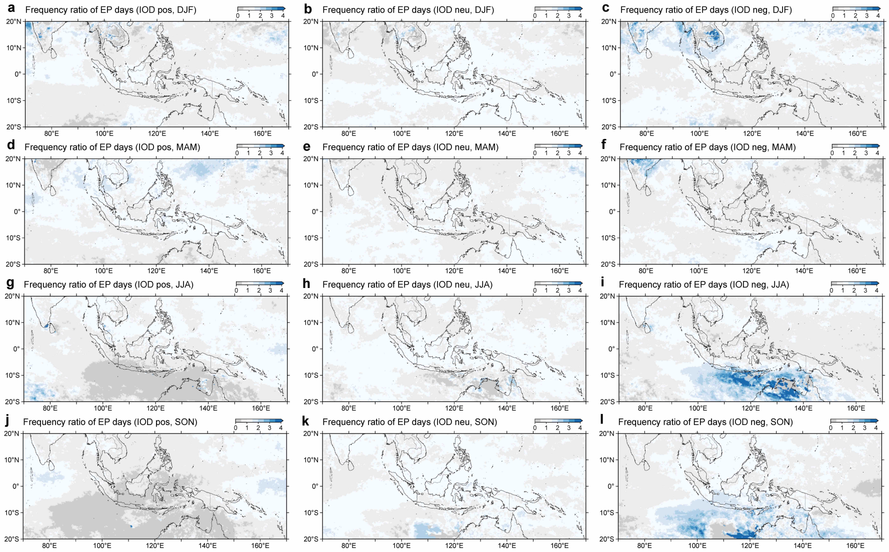

Supplementary Fig. 29: **Frequency ratio maps of extreme precipitation conditioned to different IOD phases**. The positive, negative and neutral phases were obtained using the quantile-based thresholds presented in Supplementary Information section 4.

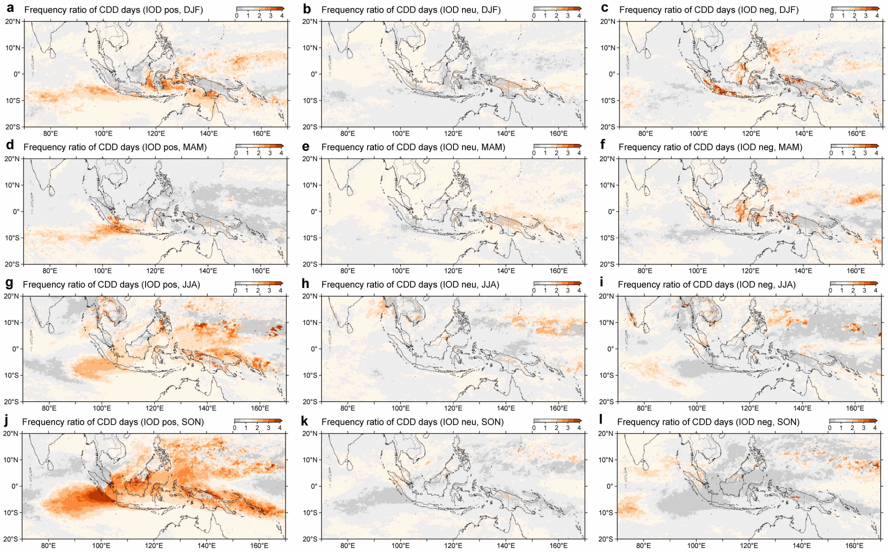

Supplementary Fig. 30: **Frequency ratio maps of consecutive dry days conditioned to different IOD phases**. The positive, negative and neutral phases were obtained using the quantile-based thresholds presented in Supplementary Information section 4.

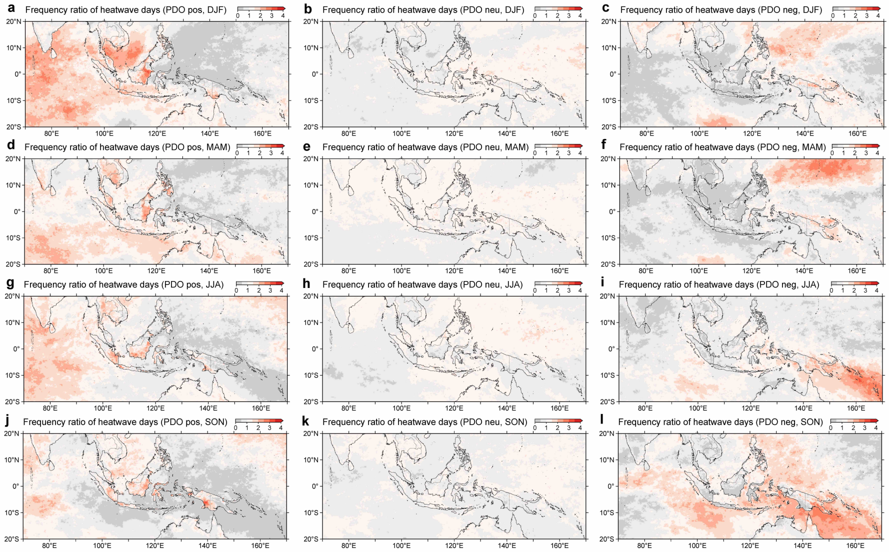

Supplementary Fig. 31: **Frequency ratio maps of heatwaves conditioned to different PDO phases**. The positive, negative and neutral phases were obtained using the quantile-based thresholds presented in Supplementary Information section 4.

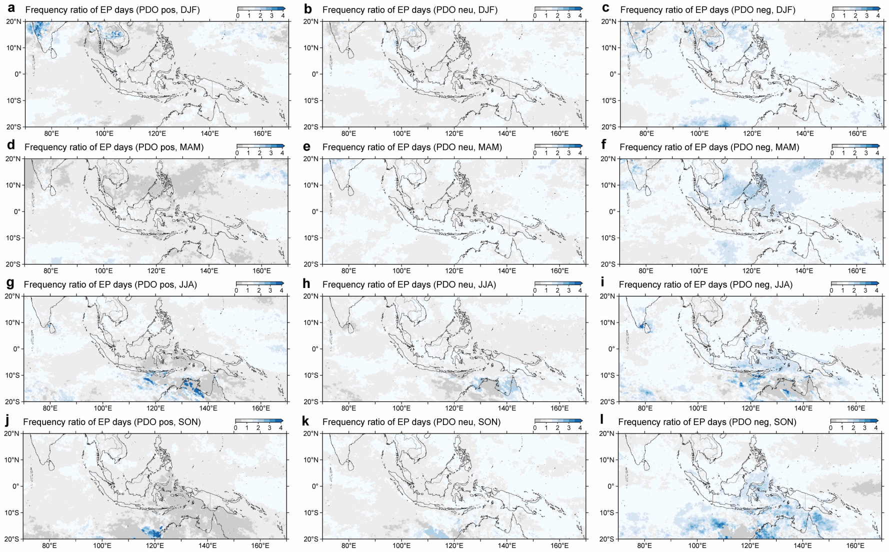

Supplementary Fig. 32: **Frequency ratio maps of extreme precipitation conditioned to different PDO phases**. The positive, negative and neutral phases were obtained using the quantile-based thresholds presented in Supplementary Information section 4.

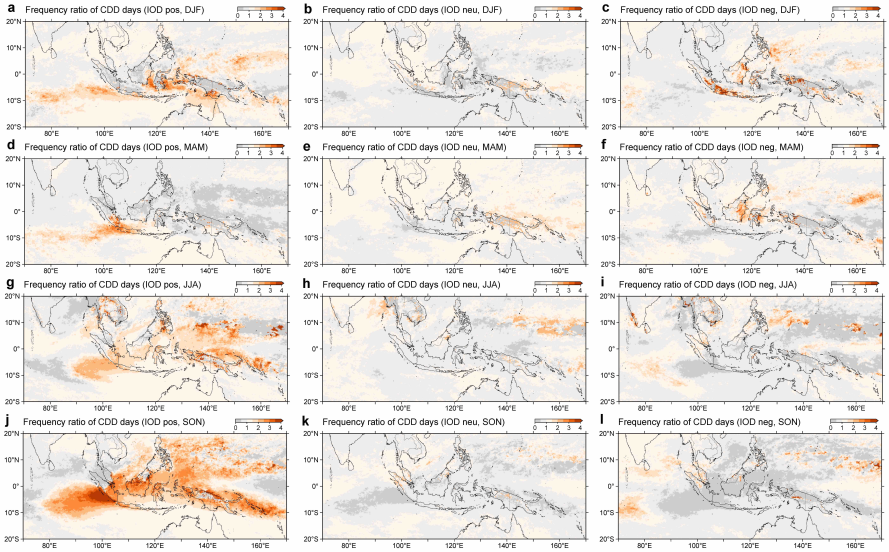

Supplementary Fig. 33: **Frequency ratio maps of consecutive dry days conditioned to different PDO phases**. The positive, negative and neutral phases were obtained using the quantile-based thresholds presented in Supplementary Information section 4.

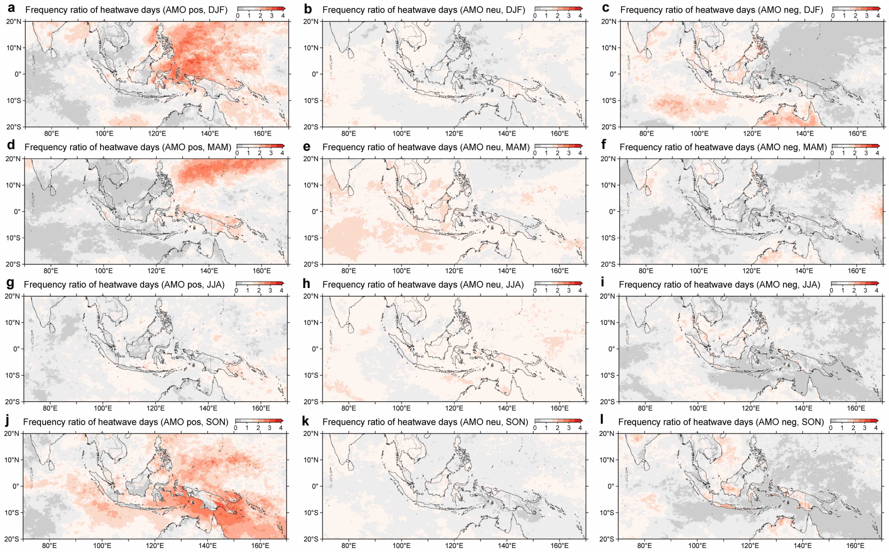

Supplementary Fig. 34: **Frequency ratio maps of heatwaves conditioned to different AMO phases**. The positive, negative and neutral phases were obtained using the quantile-based thresholds presented in Supplementary Information section 4.

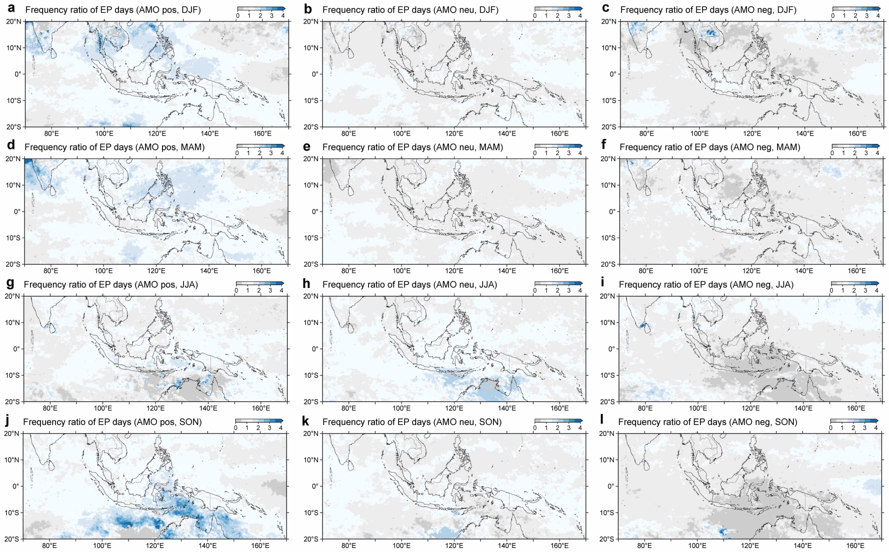

Supplementary Fig. 35: **Frequency ratio maps of extreme precipitation conditioned to different AMO phases**. The positive, negative and neutral phases were obtained using the quantile-based thresholds presented in Supplementary Information section 4.

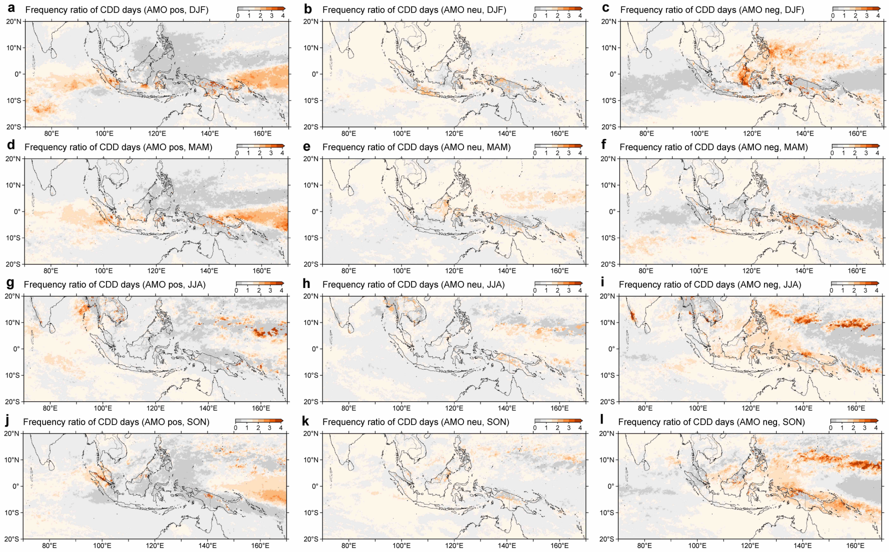

Supplementary Fig. 36: **Frequency ratio maps of consecutive dry days conditioned to different AMO phases**. The positive, negative and neutral phases were obtained using the quantile-based thresholds presented in Supplementary Information section 4.

6 Regional impacts of weather extremes associated with emerging weather patterns

In the manuscript, we analyzed weather extremes defined over the entire region, including both land and ocean. We found that the emerging weather patterns are favoring the occurrence of heatwaves and extreme precipitation events in this region. Thus, we apply various regional masks to better understand the local impacts brought by the identified emerging weather patterns. In addition to the entire region, land-only and ocean-only masks, we divided the land into 8 different regions as shown in Supplementary Fig. 37.

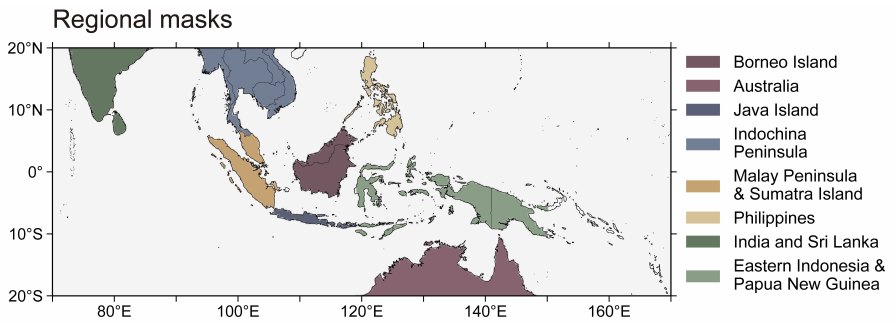

Supplementary Fig. 37: **Regional masks that are used in this study**.

For each given region, we first define local extremes following the same method described in the main text. Specifically, extreme events are identified as days when the number of grid points classified as extremes exceeds the top 10th percentile. We count the number of extreme events that are associated with emerging weather patterns and display them as the first value in each cell in Supplementary Tabs. 1 and 2. We additionally compute the frequency ratio between emerging weather patterns and climatology, showing them in parenthesis in the Supplementary Tabs. 1 and 2. The results further confirm that emerging weather patterns are bringing more heatwaves and extreme precipitation events and less dry-day events to the region in general, despite some regional and seasonal uncertainties.

7 Example of weather pattern and associated extreme

In our study, 'weather patterns' refer to specific synoptic configurations over the tropical Indo-Pacific region. More specifically, they are defined as daily mean fields of certain observables, such as Total Column Water Vapor (TCWV) and the 850hPa streamfunction. These patterns hold crucial information for the weather over the region and are linked to weather extremes,

Region	Extremes	DJF	MAM	JJA	SON
Entire region	Heatwave	33 (2.54)	23 (4.11)	16 (4.10)	16 (2.90)
	Extreme precipitation	42 (3.24)	23 (4.11)	5 (1.28)	23 (4.18)
	Dry-day event	0 (0.00)	1 (0.18)	1 (0.26)	0 (0.00)
Land	Heatwave	7 (0.54)	10 (1.78)	8 (2.05)	3 (0.54)
	Extreme precipitation	33 (2.55)	16 (2.86)	10 (2.56)	18 (3.30)
	Dry-day event	1 (0.08)	0 (0.00)	0 (0.00)	0 (0.00)
Ocean	Heatwave	35 (2.69)	23 (4.11)	16 (4.10)	16 (2.91)
	Extreme precipitation	43 (3.26)	23 (4.11)	4 (1.03)	23 (4.18)
	Dry-day event	0 (0.08)	1 (0.18)	1 (0.26)	0 (0.00)
Indochina Peninsula	Heatwave	7 (0.54)	9 (1.61)	6 (1.54)	1 (0.18)
	Extreme precipitation	41 (3.25)	11 (1.97)	3 (0.77)	8 (1.46)
	Dry-day event	1 (0.08)	1 (0.18)	3 (0.80)	5 (0.91)
India and LK	Heatwave	20 (1.54)	10 (1.78)	1 (0.26)	10 (1.82)
	Extreme precipitation	37 (2.86)	2 (0.36)	10 (2.56)	9 (1.64)
	Dry-day event	13 (1.01)	2 (0.36)	1 (0.26)	6 (1.09)

Supplementary Tab. 1: Regional impacts of weather extremes

including heatwaves, extreme precipitation events, and consecutive dry conditions. In Fig. 38 (a), we show an example of TCWV anomaly field, namely the weather pattern, at 2013/06/20. The spatial distribution of three different types of extremes at that day is shown in Fig. 38 (b, c, d), with a value of 1 indicating the occurrence of extremes and 0 denoting neutral conditions. We observe that Sumatra Island, Borneo Island, and the surrounding regions are experiencing hotter and drier conditions, primarily due to the lack

Region	Extremes	DJF	MAM	JJA	SON
Australia	Heatwave	2 (0.15)	14 (2.50)	8 (2.06)	0 (0.00)
	Extreme precipitation	18 (1.39)	5 (0.90)	1 (0.74)	12 (2.27)
	Dry-day event	3 (0.23)	0 (0.00)	0 (0.00)	0 (0.00)
Borneo Island	Heatwave	20 (1.54)	4 (0.71)	6 (1.55)	5 (0.91)
	Extreme precipitation	20 (1.54)	13 (2.34)	10 (2.58)	11 (2.00)
	Dry-day event	0 (0.00)	0 (0.00)	0 (0.00)	0 (0.00)
Java Island	Heatwave	5 (0.39)	5 (0.90)	6 (1.57)	1 (0.18)
	Extreme precipitation	17 (1.31)	8 (1.49)	12 (3.38)	14 (2.57)
	Dry-day event	6 (0.48)	6 (1.08)	0 (0)	0 (0)
Malay Peninsula and Sumatra	Heatwave	20 (1.55)	6 1.08)	0 (0.00)	10 (1.8)
	Extreme precipitation	23 (1.78)	9 (1.63)	9 (2.53)	14 (2.59)
	Dry-day event	3 (0.23)	1 (0.18)	0 (0.00)	7 (1.28)
Philippines	Heatwave	12 (0.93)	4 (0.72)	3 (0.77)	5 (0.92)
	Extreme precipitation	30 (2.33)	12 (2.22)	4 (1.05)	17 (3.14)
	Dry-day event	0 (0.00)	1 (0.18)	0 (0.00)	0 (0.00)
Eastern Indonesia and PG	Heatwave	16 (1.24)	21 (3.75)	11 (2.85)	4 (0.73)
	Extreme precipitation	24 (1.86)	10 (1.80)	6 (1.54)	13 (2.36)
	Dry-day event	5 (0.40)	0 (0.00)	1 (0.26)	0 (0.00)

Supplementary Tab. 2: Regional impacts of weather extremes

of water vapor in the atmosphere. Additionally, we noted extreme precipitation occurring to the west of the Philippines; this is attributed to a tropical depression

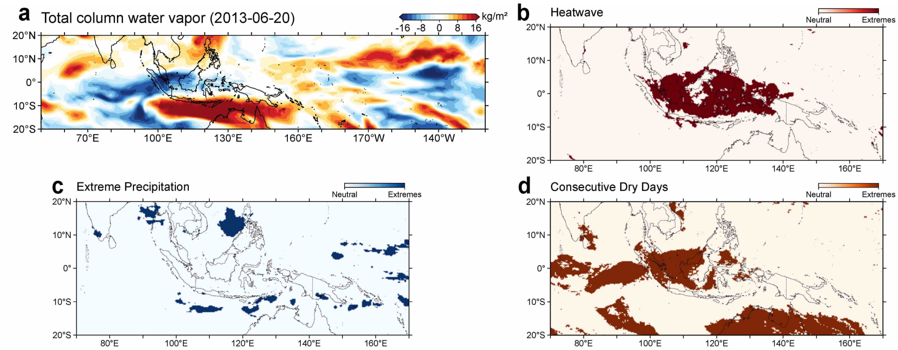

Supplementary Fig. 38: **Example of weather pattern at 2013/06/20 and associated extreme.** Daily total column water vapor anomaly at 2013/06/20 (a), and associated spatial distribution of heatwaves (b), extreme precipitation (c), and consecutive dry days (d). Grid points that are identified experiencing extremes are colored, while the others are not.

8 Importance of the study and competing work

In this last section of Supplementary Material, we detail some additional points explaining the importance of understanding changes in atmospheric weather patterns in the tropical Indo-Pacific region, and highlight existing competing work.

8.1 Importance of Indo-Pacific climate and ongoing debates

The Indo-Pacific region encompasses the tropical Pacific Ocean and the Indian Ocean. Because of this confluence, the weather of this region is modulated by the complex interaction of multiple climate drivers, including El Niño Southern Oscillation (ENSO) [7, 8], the Indian Ocean Dipole (IOD) [9, 10], the Madden Julian Oscillation (MJO) [11–13], and seasonal monsoons [14, 15], among others. These climate drivers, and their interplay with the tropical Indo-Pacific weather have far-reaching implications, and lead to weather modulation and extreme weather events in other regions of the planet [16–18].

The characterization of changes in atmospheric circulation patterns of the tropical Indo-Pacific region along with their causes have drawn the attention of several research groups worldwide. While some consensus has been reached, many results remain inconclusive, fueling uncertainty on future weather patterns, and especially weather extremes in the region. Atmospheric circulation patterns may be understood as a set of spatial patterns of a given atmospheric variable which repeatedly occur in conjunction with specific classes of weather patterns and extreme weather events.

One of the most prominent features in the tropics is the east-west atmospheric circulation over the tropical Pacific, namely the Pacific Walker Circulation (PWC). This circulation consists of rising air motion over Southeast Asia and its surrounding Oceans, namely the Indian Ocean and the western Pacific, and descending air motion over the eastern Pacific. The PWC is a crucial component of the global atmospheric circulation, and is closely connected to ENSO. Because of its potential to influence weather patterns well beyond the Indo-Pacific region, understanding how PWC changes under global warming is a critical piece in understanding future global climate. Past studies have reached different conclusions regarding changes in PWC. Some studies observed a weakened PWC [19–21], whereas most recent studies found a strengthened PWC [22–26]. Today, the community seems to have reached consensus on the strengthening of PWC. Yet, whether this strengthening is due to anthropogenic forcing or internal variability remains a subject of lively debate [27, 28].

Some model-based studies suggest that this phenomenon can be attributed to internal variability [22, 29, 30]. However, the inability of the majority of general circulation models (GCMs) in CMIP5 and CMIP6 to reproduce the strengthening of PWC raises concerns [31, 32]. Indeed, some studies suggest that PWC strengthening is driven by anthropogenic forcing and that current climate models may contain a *cold-tongue* bias in the Pacific that undermines climate projections for the region [33, 34].

Besides changes in PWC, other mechanisms may also drive changes of tropical weather patterns. A link was found between the expansion of the Indo-Pacific warm pool and the changes of MJO life cycle, increasing the residence time of MJO over the Maritime Continent [18]. Studies also suggest that Indian and Atlantic Oceans' warming [25, 31], multidecadal internal variability in the Atlantic [35], and eruptions of major volcanoes [35] can contribute to weather changes in the tropics. The focus of this study is on the intersection between the changing large-scale atmospheric circulation in the tropics, i.e., the strengthening of PWC, and its implications for weather patterns and extremes.

To this end, it is crucial to identify their underlying climate drivers, and their link to the changing atmospheric dynamics and circulation. Indeed, given the inherent complexity of the tropical Indo-Pacific climate, disentangling the relative roles of anthropogenic forcing and internal variability on the changing weather patterns in the tropics remains an open and daunting task.

8.2 Competing work on weather extremes in the Indo-Pacific

Recent observations point to more frequent and intense extreme weather events in the tropical Indo-Pacific region, especially in Southeast Asia. These include heat waves, extreme precipitation and lack thereof, that are leading to life-threatening temperatures, flooding and droughts [36–38]. For instance, using various observation and reanalysis datasets, heat waves were found to be more frequent, more persistent, and more intense in most parts of South-east Asia [39]. Using statistical trend analyses, [40] found significant changes of precipitation extremes during 1981–2017 over Southeast Asia. Although these studies have provided valuable insights into regional climate changes in the tropical Indo-Pacific region, and Southeast Asia in particular, the link between individual circulation patterns with specific weather patterns and extremes have not been comprehensively investigated. Indeed, the majority of the research efforts in this area have focused on the average atmospheric circulation state and how its change affects the frequency and intensity of extreme weather events. Ensemble-model-based projections of precipitation extremes in Southeast Asia also found increasing extremes, albeit these vary across regions, seasons and warming scenarios, suggesting a high-level of uncertainty on future changes [41]. Characterizing the climate and atmospheric drivers underlying extreme weather events is essential to understand their future behaviour and equip policy makers with valuable tools to implement effective climate resilience strategies.

References

[1] Li, J., Liang, C., Tang, Y., Dong, C., Chen, D., Liu, X., Jin, W.: A new dipole index of the salinity anomalies of the tropical indian ocean. Scientific Reports **6**(1), 24260 (2016)

[2] Scoccimarro, E., Villarini, G., Gualdi, S., Navarra, A.: The pacific decadal oscillation modulates tropical cyclone days on the interannual timescale in the north pacific ocean. Journal of Geophysical Research: Atmospheres **126**(15), 2021–034988 (2021)

[3] Apaéstegui, J., Cruz, F.W., Sifeddine, A., Vuille, M., Espinoza, J., Guyot, J.-L., Khodri, M., Strikis, N., Santos, R., Cheng, H., *et al.*: Hydroclimate variability of the northwestern amazon basin near the andean foothills of peru related to the south american monsoon system during the last 1600 years. Climate of the Past **10**(6), 1967–1981 (2014)

[4] Wang, S., Huang, J., He, Y., Guan, Y.: Combined effects of the pacific decadal oscillation and el nino-southern oscillation on global land dry–wet changes. Scientific reports **4**(1), 6651 (2014)

[5] McCabe, G.J., Palecki, M.A., Betancourt, J.L.: Pacific and atlantic ocean influences on multidecadal drought frequency in the united states. Proceedings of the National Academy of Sciences **101**(12), 4136–4141 (2004)

[6] Hanley, D.E., Bourassa, M.A., O'Brien, J.J., Smith, S.R., Spade, E.R.: A quantitative evaluation of enso indices. Journal of Climate **16**(8), 1249–1258 (2003)

[7] Villafuerte, M.Q., Matsumoto, J.: Significant influences of global mean temperature and enso on extreme rainfall in southeast asia. Journal of Climate **28**(5), 1905–1919 (2015)

[8] Räsänen, T.A., Lindgren, V., Guillaume, J.H., Buckley, B.M., Kummu, M.: On the spatial and temporal variability of enso precipitation and drought teleconnection in mainland southeast asia. Climate of the Past **12**(9), 1889–1905 (2016)

[9] Saji, N., Yamagata, T.: Possible impacts of indian ocean dipole mode events on global climate. Climate Research **25**(2), 151–169 (2003)

[10] Vinayachandran, P., Francis, P., Rao, S.: Indian ocean dipole: processes and impacts. Current trends in science **46**(10), 569–589 (2009)

[11] Zhang, C.: Madden-julian oscillation. Reviews of Geophysics **43**(2) (2005)

[12] Xavier, P., Rahmat, R., Cheong, W.K., Wallace, E.: Influence of madden-julian oscillation on southeast asia rainfall extremes: observations and predictability. Geophysical Research Letters **41**(12), 4406–4412 (2014)

[13] Da Silva, N.A., Matthews, A.J.: Impact of the madden–julian oscillation on extreme precipitation over the western maritime continent and south-east asia. Quarterly Journal of the Royal Meteorological Society **147**(739), 3434–3453 (2021)

[14] Lau, K., Yang, S.: Climatology and interannual variability of the southeast asian summer monsoon. Advances in Atmospheric Sciences **14**, 141–162 (1997)

[15] Loo, Y.Y., Billa, L., Singh, A.: Effect of climate change on seasonal monsoon in asia and its impact on the variability of monsoon rainfall in southeast asia. Geoscience Frontiers **6**(6), 817–823 (2015)

[16] Molteni, F., Stockdale, T.N., Vitart, F.: Understanding and modelling extra-tropical teleconnections with the indo-pacific region during the northern winter. Climate dynamics **45**, 3119–3140 (2015)

[17] Feba, F., Ashok, K., Ravichandran, M.: Role of changed indo-pacific atmospheric circulation in the recent disconnect between the indian summer monsoon and enso. Climate Dynamics **52**, 1461–1470 (2019)

[18] Roxy, M., Dasgupta, P., McPhaden, M.J., Suematsu, T., Zhang, C., Kim, D.: Twofold expansion of the indo-pacific warm pool warps the mjo life cycle. Nature **575**(7784), 647–651 (2019)

[19] Vecchi, G.A., Soden, B.J., Wittenberg, A.T., Held, I.M., Leetmaa, A., Harrison, M.J.: Weakening of tropical pacific atmospheric circulation due

to anthropogenic forcing. Nature **441**(7089), 73–76 (2006)

[20] Tokinaga, H., Xie, S.-P., Deser, C., Kosaka, Y., Okumura, Y.M.: Slowdown of the walker circulation driven by tropical indo-pacific warming. Nature **491**(7424), 439–443 (2012)

[21] Power, S.B., Kociuba, G.: What caused the observed twentieth-century weakening of the walker circulation? Journal of Climate **24**(24), 6501–6514 (2011)

[22] England, M.H., McGregor, S., Spence, P., Meehl, G.A., Timmermann, A., Cai, W., Gupta, A.S., McPhaden, M.J., Purich, A., Santoso, A.: Recent intensification of wind-driven circulation in the pacific and the ongoing warming hiatus. Nature climate change **4**(3), 222–227 (2014)

[23] Takahashi, C., Watanabe, M.: Pacific trade winds accelerated by aerosol forcing over the past two decades. Nature Climate Change **6**(8), 768–772 (2016)

[24] Sohn, B., Yeh, S.-W., Schmetz, J., Song, H.-J.: Observational evidences of walker circulation change over the last 30 years contrasting with gcm results. Climate Dynamics **40**, 1721–1732 (2013)

[25] McGregor, S., Timmermann, A., Stuecker, M.F., England, M.H., Merrifield, M., Jin, F.-F., Chikamoto, Y.: Recent walker circulation strengthening and pacific cooling amplified by atlantic warming. Nature Climate Change **4**(10), 888–892 (2014)

[26] Ma, S., Zhou, T.: Robust strengthening and westward shift of the tropical pacific walker circulation during 1979–2012: A comparison of 7 sets of reanalysis data and 26 cmip5 models. Journal of Climate **29**(9), 3097–3118

(2016)

[27] Heede, U.K., Fedorov, A.V., Burls, N.J.: Time scales and mechanisms for the tropical pacific response to global warming: A tug of war between the ocean thermostat and weaker walker. Journal of Climate **33**(14), 6101–6118 (2020)

[28] Heede, U.K., Fedorov, A.V., Burls, N.J.: A stronger versus weaker walker: understanding model differences in fast and slow tropical pacific responses to global warming. Climate Dynamics **57**(9-10), 2505–2522 (2021)

[29] Chung, E.-S., Timmermann, A., Soden, B.J., Ha, K.-J., Shi, L., John, V.O.: Reconciling opposing walker circulation trends in observations and model projections. Nature Climate Change **9**(5), 405–412 (2019)

[30] Douville, H., Voldoire, A., Geoffroy, O.: The recent global warming hiatus: What is the role of pacific variability? Geophysical Research Letters **42**(3), 880–888 (2015)

[31] Kociuba, G., Power, S.B.: Inability of cmip5 models to simulate recent strengthening of the walker circulation: Implications for projections. Journal of Climate **28**(1), 20–35 (2015)

[32] Coats, S., Karnauskas, K.: Are simulated and observed twentieth century tropical pacific sea surface temperature trends significant relative to internal variability? Geophysical Research Letters **44**(19), 9928–9937 (2017)

[33] Kohyama, T., Hartmann, D.L., Battisti, D.S.: La niña–like mean-state response to global warming and potential oceanic roles. Journal of Climate **30**(11), 4207–4225 (2017)

[34] Seager, R., Cane, M., Henderson, N., Lee, D.-E., Abernathey, R., Zhang, H.: Strengthening tropical pacific zonal sea surface temperature gradient consistent with rising greenhouse gases. Nature Climate Change **9**(7), 517–522 (2019)

[35] Sun, C., Kucharski, F., Li, J., Jin, F.-F., Kang, I.-S., Ding, R.: Western tropical pacific multidecadal variability forced by the atlantic multidecadal oscillation. Nature communications **8**(1), 15998 (2017)

[36] Phan-Van, T., Nguyen-Ngoc-Bich, P., Ngo-Duc, T., Vu-Minh, T., Le, P.V., Trinh-Tuan, L., Nguyen-Thi, T., Pham-Thanh, H., Tran-Quang, D.: Drought over southeast asia and its association with large-scale drivers. Journal of Climate **35**(15), 4959–4978 (2022)

[37] Dong, Z., Wang, L., Sun, Y., Hu, T., Limsakul, A., Singhruck, P., Pimonsree, S.: Heatwaves in southeast asia and their changes in a warmer world. Earth's Future **9**(7), 2021–001992 (2021)

[38] Caesar, J., Alexander, L., Trewin, B., Tse-Ring, K., Sorany, L., Vuniyayawa, V., Keosavang, N., Shimana, A., Htay, M., Karmacharya, J., *et al.*: Changes in temperature and precipitation extremes over the indo-pacific region from 1971 to 2005. International Journal of Climatology **31**(6), 791–801 (2011)

[39] Li, X.-X., Yuan, C., Hang, J.: Heat wave trends in southeast asia: comparison of results from observation and reanalysis data. Geophysical Research Letters **49**(4), 2021–097151 (2022)

[40] Fan, Y., Li, J., Zhu, S., Li, H., Zhou, B.: Trends and variabilities of precipitation and temperature extremes over southeast asia during 1981–2017.

Meteorology and Atmospheric Physics **134**(4), 78 (2022)

[41] Tangang, F., Juneng, L., Cruz, F., Chung, J.X., Ngai, S.T., Salimun, E., Mohd, M.S.F., Santisirisomboon, J., Singhruck, P., PhanVan, T., *et al.*: Multi-model projections of precipitation extremes in southeast asia based on cordex-southeast asia simulations. Environmental Research **184**, 109350 (2020)